ACS Chemical Neuroscience

Letter

N-terminal acetylation preserves #-synuclein from oligomerization by blocking intermolecular hydrogen bonds

Bing Bu, Xin Tong, Dechang Li, Yachong Hu, Wangxiao He, Chunyu Zhao, Rui Hu, Xiaoqing Li, Yongping Shao, Cong Liu, Qing Zhao, Baohua Ji, and Jiajie Diao

ACS Chem. Neurosci., **Just Accepted Manuscript** • DOI: 10.1021/acschemneuro.7b00250 • Publication Date (Web): 25 Jul 2017

ACS Publications

ACS Chemical Neuroscience is published by the American Chemical Society. 1155 Sixteenth Street N.W., Washington, DC 20036

N-terminal acetylation preserves α-synuclein from oligomerization by blocking intermolecular hydrogen bonds

Bing Bu[1*], Xin Tong[2*], Dechang Li[1†], Yachong Hu[3,4], Wangxiao He[4], Chunyu Zhao[5], Rui Hu[2], Xiaoqing Li[2], Yongping Shao[4], Cong Liu[5], Qing Zhao[2†], Baohua Ji[1†], and Jiajie Diao[3†]

1. Biomechanics and Biomaterials Laboratory, Department of Applied Mechanics, Beijing Institute of Technology, Beijing 100081, China.
2. State Key Laboratory for Mesoscopic Physics and Electron Microscopy Laboratory, School of Physics, Peking University, Beijing 100871, China.
3. Department of Cancer Biology, University of Cincinnati College of Medicine, Cincinnati, OH 45267, USA.
4. Key Laboratory of Biomedical Information Engineering of the Ministry of Education, School of Life Science and Technology, Xi'an Jiaotong University, Xi'an 710049, China.
5. Interdisciplinary Research Center on Biology and Chemistry, Shanghai Institute of Organic Chemistry, Chinese Academy of Sciences, Shanghai 200032, China.

ABSTRACT

The abnormal aggregation of α-synuclein (α-Syn) is closely associated with Parkinson's diseases.

Different post-translational modifications of α-Syn have been identified and contribute distinctly in α-Syn aggregation and cytotoxicity. Recently, α-Syn was reported to be N-terminally acetylated in cell, yet the functional implication of this modification, especially in α-Syn oligomerization remains unclear. By using a solid-state nanopore system, we found that N-terminal acetylation can significantly decrease α-Syn oligomerization. Replica-exchange molecular dynamics simulations further revealed that addition of acetyl group at the N-terminus disrupts intermolecular hydrogen bonds, which slows down the initial α-Syn oligomerization. Our finding highlights the essential role of N-terminal acetylation of α-Syn in preserving its native conformation against pathological aggregation.

KEYWORDS

α-synuclein, N-terminal acetylation, Parkinson's disease oligomerization

α-Synuclein (α-Syn) is an abundant presynaptic protein expressed throughout the central nervous system (CNS). It contains a conserved lipid-binding domain and is involved in synaptic vesicle trafficking [1-5]. α-Syn aggregation is the major component of Lewy bodies which is the hallmark of Parkinson's disease, dementia with Lewy bodies, and other neurodegenerative diseases [6]. Pathologically, missense mutations (e.g. A30P, E46K, A53T) [7-9] and amplification of the α-Syn gene [10-11] are linked to early onset Parkinson's disease. α-Syn exhibits intrinsic disordered structure in aqueous solution. It has high propensity to aggregate in a nucleation-dependent manner, forming amyloid oligomers and fibrils which are cytotoxic [12-14] and are believed to contribute to neurodegeneration in Lewy body diseases. Most recently, an in-cell nuclear magnetic resonance (NMR) study showed that both the N- and C-terminal regions of α-Syn are exposed in the cytoplasm while the aggregation-prone non-amyloid-β component (NAC) region is shielded [15]. α-Syn remains as a monomer in cell [16]. Therefore, finding factors stabilizing monomeric α-Syn are of great importance to understand why α-Syn resists aggregating in cell under a high concentration. Such factors are essential for possible therapeutic targets.

Various post-translational modifications (PTMs) such as phosphorylation and acetylation have been identified on α-Syn, which may play an important functional or pathological role. Previous studies showed that N-terminal acetylation of α-Syn can stabilizes the N-terminal helicity [17] for a stronger membrane interaction [18]. Moreover, N-terminal acetylation was found to influence the aggregation of

α-Syn [19], resulting in a narrower distribution of the aggregation lag time and rates [20]. A recent simulation study [21] showed that N-terminal acetylation increased the gyration radius and reduced intramolecular hydrogen bonds of individual α-Syn monomer. However, the effect of N-terminal acetylation on the intermolecular interaction and the initial aggregation process such as small oligomer formation remains to be explored.

Here, through a label-free single molecule detection method based on solid-state nanopores, we detected a significant decrease in α-Syn oligomerization caused by N-terminal acetylation. Furthermore, through replica-exchange molecular dynamics (REMD) simulations of the oligomerization of multiple α-Syn monomers, we found that introducing acetyl group at the N-terminus of α-Syn blocks the formation of intermolecular hydrogen bonds (H-bonds) that are important for α-Syn oligomerization.

Solid-state nanopores provide a unique approach to qualitatively measure the protein oligomers of certain sizes in a fairly high resolution. As demonstrated in Figure 1A, driven by electric force, charged α-Syn oligomers suspended in solution translocate through a nanometer-scale pore imbedded in a thin membrane separating two electrolyte-filled reservoirs, resulting in ionic current drops. The statistical analysis of these ionic current drops and their persisting time can reveal the geometry and charge properties of α-Syn oligomers (Figure 1B). Mature fibrils and larger aggregations exceed the size of the nanopore are excluded while the translocation events of monomers are below the detection limit. Thus,

as demonstrated in previous publications [22-23], only small oligomers (< 8 nm) formed at the early stage of α-Syn aggregation is selectively monitored in this system.

We then used this *in situ* and label-free single-particle detection method to monitor the changes of α-Syn oligomer formed in the initial phase of α-Syn aggregation upon N-terminal acetylation. N-terminally acetylated α-Syn was prepared using a semi-synthesis approach for testing in a solid-state nanopore system (Figure S1). The current blockage distributions of N-acetylated and wild-type (WT) α-Syn were measured after a 0, 24, 48, 72-hour incubation time and the results are shown in Figure 1C-J. Figures 1C, 1E, 1G, and 1I correspond to WT α-Syn samples and Figures 1D, 1F, 1H, and 1J correspond to N-acetylated α-Syn samples, respectively. In these current blockage distributions, three types of α-Syn oligomers with different sizes were identified through multi-peak Gaussian fitting, as denoted with O_I, O_{II}, and O_{III} in Figure 1C. Detailed fitted peak positions for these three oligomers are summarized in Table S1. For instance, for the O_I peak, it positions at 0.40 pA, 0.43 pA, 0.39 pA, and 0.37 pA in 0 h, 24 h, 48 h, and 72 h wild-type samples, demonstrating a well-defined behavior. Therefore, we classify the observed populations in Figure 1C-J into three types of oligomers: O_I, O_{II}, and O_{III}. Here, we observed that the current blockage of acetylated α-Syns presents narrower distributions than those of wild-type ones (see Figure 1 C-J). The narrower current blockage distributions of acetylated α-Syns indicate more homogenous population of oligomers formed, which is consistent with previous findings [20].

The percentage of under-curve area for each Gaussian component is proportional to the number of captured molecules. Therefore, we are able to monitor the time-dependent quantity fraction of the three types of oligomers and give kinetic information of α-Syn oligomerization. The percentages of total under-curve area for O_I and O_{II} Gaussian components in 0 h, 24 h, 48 h, and 72 h have been calculated and the data is illustrated as a function of incubation time in Figure 1K and 1L. As shown in Figure 1K and 1L, for the wild-type α-Syn, oligomer I gradually decreases, while oligomer II increases persistently during the incubation. The general trend of oligomer I and II implies an aggregation process that oligomer I undergoes a continuous conversion to oligomer II. In comparison, N-terminally acetylated α-Syn remains its proportion within the 72 h incubation, which is demonstrated by a significantly reduced number of larger oligomers, indicating a decelerated oligomerization process induced by N-terminal acetylation. Oligomer III is limited to the comparatively low capture rate, and hard to analyze its aggregation character.

According to previous studies [24], the current blockage cause by protein can be described as:

$$\Delta I(t) = I_0 \frac{\Lambda(t)}{H_{eff} A_p}$$

where ΔI(t) is current blockage, I_0 is the current baseline, Λ(t) is the volume occupied by the oligomer, H_{eff} is the thickness and A_p is the cross section of nanopores. By using multi-peak Gaussian fitting of the current blockage, three types of α-Syn oligomers with increasing sizes were identified.

To gain the mechanistic insight into the prevention of large α-Syn oligomers by N-terminal acetylation, we analyzed the intermolecular dynamics of N-terminally acetylated α-Syn molecules by the REMD simulation. The REMD results showed that N-terminal acetylation can stabilize their N-terminal helicity and reduce the intramolecular H-bond numbers in oligomerization, which is consistent with previous studies of individual α-Syn simulations and experiments [17, 19, 21]. Figure 2 shows the simulation results of the radius of gyration for multiple α-Syn molecules. Simulations started with the structural model of monomeric α-Syn (PDB: 1XQ8) revealed that the gyration radius (R_g) of N-terminally acetylated α-Syn oligomers exhibit a larger average value compared to the unacetylated ones (Figure 2A and 2B). The average R_g shifted from $\overline{R}_g^{MET} = 2.76nm$ to $\overline{R}_g^{ACE} = 4.34nm$ in a three-α-Syn model and from $\overline{R}_g^{MET} = 3.45nm$ to $\overline{R}_g^{ACE} = 5.97nm$ in a five-α-Syn model, respectively. Simulations started with disordered structures gave a similar result, in which the N-terminal acetylation led to a larger R_g of multiple α-Syn molecules, as shown in Figures 2C and 2D. To compare with previous studies, we calculated the radius of gyration of individual α-Syn in oligomers (see Table S2 in Supplementary Information). It showed that the radius of gyration of individual α-Syn in oligomers with N-terminal acetylation is slightly larger than that of wild type, which is consistent with previous studies of individual α-Syn simulations [21]. In addition, we also calculated the intermolecular distances between individual α-Syn in oligomers. The average intermolecular distance for MET-N-terminal α-Syns is 3.8 ± 1.3nm. In contrast, the average intermolecular distance for ACE-N-terminal ones is 4.8

±1.8nm. The results showed that the intermolecular distance was increased by ~1nm according to the N-terminal acetylation. We can see in Table S2 that the N-terminal acetylation only enlarges the radius of gyration of individual α-Syn by about 0.01~0.04 nm. However, the radius of gyration of oligomers of ACE-N-terminal α-Syns is larger than that of MET-N-terminal ones by ~1 nm (see Figure 2). The above results indicated that the change of the oligomer radius of gyration is due to the intermolecular distance of α-Syns in N-terminal acetylation. These results suggested that the N-terminal acetylation of α-Syn may cause a weak intermolecular interaction.

We further analyzed the alteration of intermolecular H-bond network pattern during α-Syn oligomerization to address how N-terminal acetylation blocks α-Syn oligomerization. Because N-terminal acetylation induces a loss of two H-bonds donors at the N-terminus of α-Syn, we speculated that the N-terminal acetylation may disrupt the intra- and/or intermolecular H-bond network of α-Syn and impede the oligomerization process. To test this, we comparatively analyzed the H-bond numbers in the three- and five-α-Syn models of N-terminally acetylated and WT α-Syn using two different starting structures (Figures 3A and 3B). We found that the N-terminal of the wild type α-Syn can form H-bonds with residues ASP, GLU and ASN, as well as the group –C=O at the backbone, as shown in Figure S3 in the Supplementary Information. The molecular dynamics (MD) simulations confirmed that the amount of H-bonds in N-terminally acetylated three- and five-α-Syn models is significantly less than that of the WT α-Syn. More importantly, some intermolecular hydrogen bonds formed among

the N-terminus and between the N-terminus and residues in other regions are indeed blocked by the N-terminal acetylation, (Figure 3C and D), further supporting our hypothesis.

PTM has been found to commonly exist in different amyloid proteins. Depending on the modification sites and types, PTM was found to either facilitate pathological aggregation or inhibits amyloid oligomerization [25-27]. Therefore, PTM plays an essential and multifaceted role in regulating amyloid protein aggregation under different conditions. As one of the most common protein modifications, N-terminal acetylation is a major determinant of degradation signal and the functional regulation of proteins [28]. Under physiological conditions, α-Syn remains as a monomer with N-terminally acetylated in cells in an extremely high concentration of 5-50 μm/ml [15]. Previous studies suggested that the N-terminal of α-Syn is critical for α-Syn oligomerization [17-20, 29-30]. With both experimental approaches and numerical simulation, we showed that N-terminal acetylation decelerates the formation of α-Syn oligomers. We found that acetylation stabilizes the N-terminal helicity and reduces the interactions between the N-terminal and other region, which may predispose N-terminally acetylated α-Syn toward specific interactions with others and decrease nonspecific interactions to form various oligomers to service as aggregation seeds. The reduction of inhomogeneous oligomers may lead to a slower aggregation time of N-terminally acetylated α-Syns than those of non-acetylated ones [19-20]. The formation of small oligomers at the initial phase of protein aggregation is believed to play an essential role in pathogenesis, such as dimer and trimer of amyloid-β in Alzheimer's Diseases [31]. Since α-Syn

aggregations are highly toxic *in vivo* and is closely associated with early onset of Parkinson's disease pathology [32-34], this study suggests the oligomerization-mediated toxicity of α-Syn might be alleviated by the N-terminal acetylation.

Due to unstable and transit properties of amyloid oligomers, it remains changeling to probe the structural changes in amyloid oligomer formation at atomic level experimentally. Although it has been found that N-terminal acetylation loose the structure of individual α-Syn monomer [21], few studies showed the impact of N-terminal acetylation on the intermolecular interaction in the formation of small α-Syn oligomer. By combining nanopore detection and MD simulations, we found the molecular mechanism of N-terminal acetylation of α-Syn in decelerating small oligomer formation. In the solid-state nanopore detection experiment, we noticed more large blockages corresponding to bigger oligomers of the unacetylated α-Syn (see the arrows in Figures 1C and 1D), indicating that the N-terminally acetylated α-Syn has a slower oligomerization process. It is known that the H-bond network is critical to stabilize the protein-protein interactions [35-39]. Our simulations showed that the H-bond network of the N-terminally acetylated α-Syn oligomers was disrupted by acetylation of the N-terminus, destabilizing the oligomerization state of α-Syn.

METHODS

Semisynthesis of N-terminally acetylated α-Syn

The ACE-α-Syn(1-18)-SR (R=CH2CH2SO3H) peptide was synthesized on an CSbio 336X automated peptide synthesizer using the optimized HBTU (2-(1H-benzotriazol-1-yl)-1,1,3,3-tetramethyluronium hexafluorophosphate) activation/DIEA (N,N-Diisopropylethylamine) in situ neutralization protocol for Boc-chemistry solid phase peptide synthesis. The initial loading was performed by coupling with S-trityl protected mercaptopropionic acid. After cleavage and deprotection in HF, crude products were precipitated with cold ether and purified to homogeneity by preparative C18 reversed-phase high performance liquid chromatography (HPLC). The molecular masses were ascertained by electrospray ionization mass spectrometry.

Native chemical ligation, desulfurization, and purification

α-Syn Δ1-18 A19C was treated with 100 mM O-methylhydroxylamine and 30 eq of tris (2-carboxyethyl) phosphine (TCEP) in 6 M GdnHCl at pH 4.0 for 12 h at room temperature. The protein was then separated from the reagents and by-products by reversed-phase HPLC, lyophilized, and stored at -20 ^{o}C under inert atmosphere until use. For large scale ligations, α-Syn Δ1-18 A19C was dissolved in 1 ml of 6 M GdnHCl, 0.2 M sodium phosphate to a final concentration of 0.83 mM. 30 eq of TCEP were added to prevent disulfide formation. 1.2 eq of ACE-α-Syn(1-18)-SR were added, followed by 10 eq of 4-mercaptophenylacetic acid (with respect to the peptide fragment) as the NCL catalyst. The pH was then adjusted to 7.0 with aqueous NaOH, and the reaction was incubated at 37 ^{o}C under inert atmosphere for up to 4 h. The ligation product was purified by reversed-phase HPLC on a

semipreparative Waters C4 column, evaporated, and lyophilized. After lyophilization, the powder was redissolved in 1ml of 6 M GdnHCl, 0.2 M sodium phosphate, pH 7.0. To this solution, 1 ml of 1.0 M TCEP in 6 M GdnHCl, pH 7.0, t-butyl mercaptan was added to a final concentration of 840 mM, and VA-044 to a final concentration of 5.4 mM. The reaction proceeded for 2 h, and the final product was purified to homogeneity by preparative C4 RP-HPLC.

Nanopore detection

The chips containing solid-state nanopores were installed in a sealed fluid cell and separated into two electrically isolated reservoirs of electrolytes. The tween 20 coating buffer diluted protein sample was introduced into the *cis* side of the fluid cell. The voltage was applied through two Ag/AgCl electrodes coupled to the two opposite electrolyte reservoirs by an Axon 200B patch clamp amplifier (Molecular Devices, Sunnyvale, CA). Attached with an 8-pole, 100kHz, low pass Bessel filter operating in resistive feedback mode, the patch clamp was also used for ionic current measurement. The output of the patch clamp was digitized at 250 kHz and continuously recorded by an Axon Digidata 1440A digitizer and pClamp 10.3 software, and then analyzed through custom MATLAB code (The MathWorks, Natick, MA). All the events showed in the figures were filtered by a 40kHz low-pass Bessel filter through MATLAB code for clarity.

Simulation models

Enhanced sampling molecular simulations of oligomerization of human α-Syn were performed in N-terminal acetylated state (i.e., the ACE-N-terminal state) and non-acetylated state (i.e., the MET-N-terminal state). In the ACE-N-terminal state, the N-terminus of α-Syn undergoes N-terminal acetylation with an acetyl group (-CO-CH_3), while in the non-acetylated state, α-Syn ended with an amino group (-NH_3). As well known, α-Syn exhibits intrinsic disordered structure in aqueous solution [15]. In contrast, α-Syn may form helix structure with association of phospholipid membrane [40-41]. To study the secondary structure effect in the oligomerization process, two types of initial structures were used. One initial structure started with the structure (PDB: 1XQ8) [40] with two α-helices in each α-Syn (see Model I in Figure S2 (A) and (B)). The second initial structure (Model II in Figure S2 (C) and (D)) started with a disordered coiled structure based on the sequence in each α-Syn. To study the concentration effect of α-Syn in oligomerization, three or five α-Syn molecules were randomly put in a 13×13×13 nm^3 cubic simulation box. In the beginning, the distance between each α-Syn was larger than 10 Å so that there was no contact between individual α-Syn (see Figure S2).

Replica-exchange molecular dynamics simulation

Replica-exchange molecular dynamics (REMD) simulations [42-44] were applied to enhance the sampling of the oligomerization structure of α-Syn molecules. The CHARMM36 force field [45-46] was used and periodic boundary condition was applied. Implicit solvent model with the Generalized Born Surface Area (GBSA) method [47] was employed in the simulations. The GBSA implicit solvent method is

widely used in the study of protein-protein interactions and protein folding simulations [48-52]. Non-bonded interactions were calculated with a cut-off of 12 Å. All bond lengths were constrained with the LINCS algorithm [53] and a time step of 2 fs was set. Temperature for each simulation was achieved by coupling the system with a V-rescale thermostat. For REMD simulations, 30 replicas for the three-α-Syn system and 38 replicas for the five one were performed, respectively, and each replica ran for 50 ns in the temperature range from 300K to 550K, resulting to a total simulation time of 1500 ns and 1900 ns for the three-α-Syn system and the five one, respectively. The REMD simulations were conducted using GROMACS 5.0.7 [54-55] software package. Trajectories with the lowest temperature 300 K were used for data collection and analysis.

The radius of gyration of the oligomerization structure R_g is calculated by,

$$R_g = \left(\frac{\sum_i m_i \left\| r_i \right\|^2}{\sum_i m_i} \right)^{\frac{1}{2}} \quad (1)$$

where m_i is the mass of atom *i*, and r_i is the position of atom *i* with respect to the center of mass of the molecule. The radius of gyration has been shown to accurately describe the oligomerization state of multiple proteins [15, 21, 56].

To determine whether a H-bond exists between a donor and acceptor associated with the N-terminus of α-Syn, a geometrical criterion was adopted in which the formation of a hydrogen bond was defined by

both atom distance and bond orientation. For instance, the donor D, hydrogen H, and acceptor A with a D-H…A configuration was regarded as a hydrogen bond when the distance between donor D and acceptor A was shorter than 3.5 Å and the bond angle of H-D…A was smaller than 30°.

AUTHOR INFORMATION

Corresponding Authors

†Email addresses: dcli@bit.edu.cn, zhaoqing@pku.edu.cn, bhji@bit.edu.cn, and jiajie.diao@uc.edu

Author Contributions

*These authors contributed equally. Q.Z., B.J., and J.D. contributed to experiment concept and design. B.B. and D.L. performed molecular dynamics simulations. T.X., R.H., X.L., and Q.Z. acquired and analyzed data for nanopore experiments. W.H., C.Z., Y.H., Y.S., and C.L. synthesized wild-type α-Syn and α-Syn with N-terminal acetylation. D.L., C.L., B.J., and J.D. wrote manuscript.

Funding

This work was supported by funds from 973-projects (2015CB856304, 2013CB932602) and 863-program (2015AA020907) from Ministry of Science and Technology, China, and National Natural Science Foundation of China (NSFC 51622201, 61571015, 11372042, 11532009, 11521062).

Notes

The authors declare no competing financial interest.

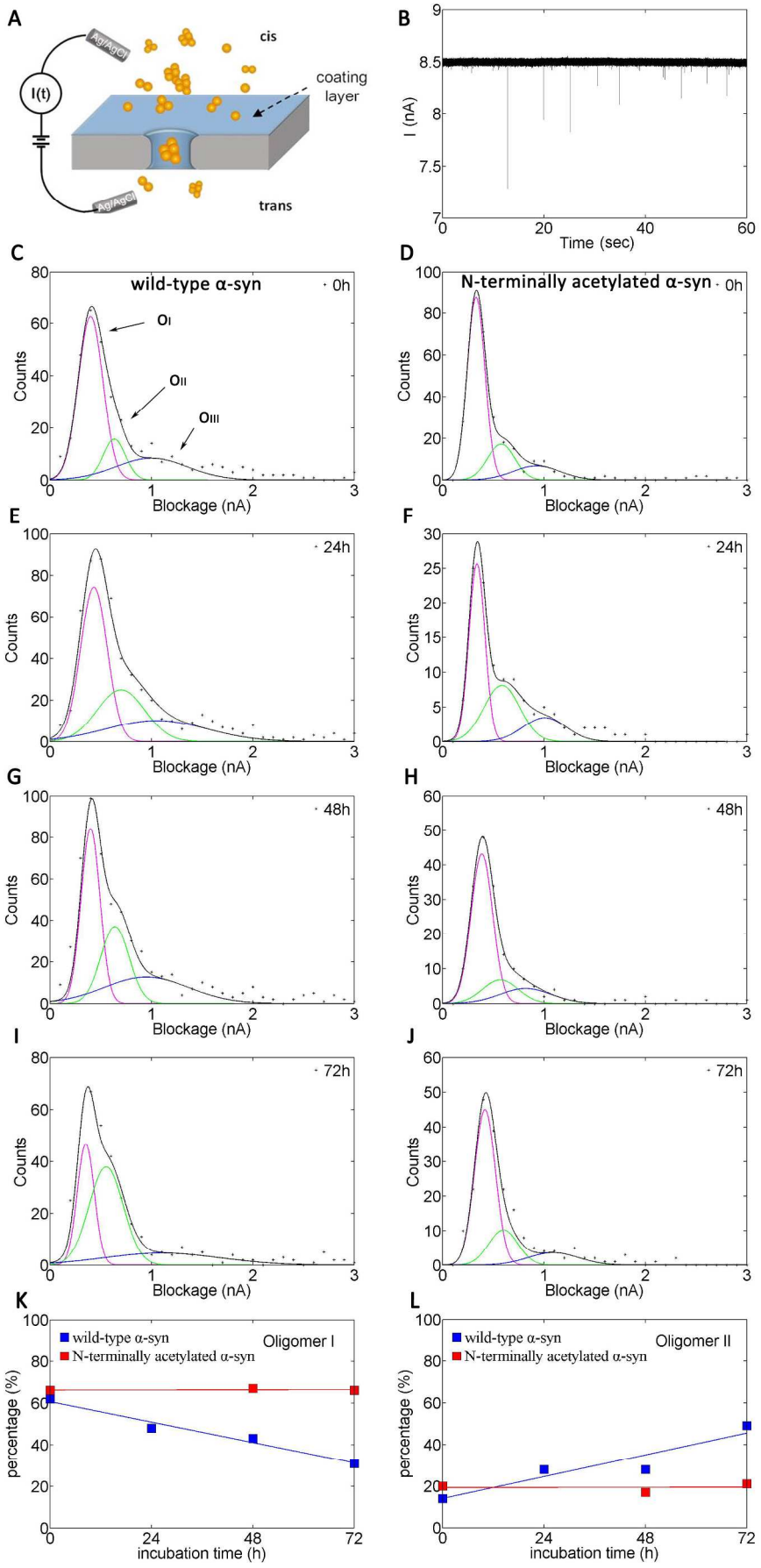
A
Ag/AgCl
cis
I(t)
coating layer
trans
Ag/AgCl
B
I (nA)
Time (sec)
C
wild-type α-syn
0h
OI
OII
OIII
Counts
Blockage (nA)
D
N-terminally acetylated α-syn
0h
Counts
Blockage (nA)
E
24h
Counts
Blockage (nA)
F
24h
Counts
Blockage (nA)
G
48h
Counts
Blockage (nA)
H
48h
Counts
Blockage (nA)
I
72h
Counts
Blockage (nA)
J
72h
Counts
Blockage (nA)
K
wild-type α-syn
N-terminally acetylated α-syn
Oligomer I
percentage (%)
incubation time (h)
L
wild-type α-syn
N-terminally acetylated α-syn
Oligomer II
percentage (%)
incubation time (h)

Figure 1. (A) Schematic diagram of experimental setup. The flow cell is separated by a silicon nitride membrane with a solid-state nanopore embedded on it. To provide a non-specific adsorption surface, the silicon nitride membrane is coated by a layer of tween 20 molecules (light blue layer) [57]. (B) A current trace of nanopore experiment under 100 mV. Current blockage histograms with Gaussian fitting (pink, green, and blue lines) for 0, 24, 48 and 72 h incubation of wild-type α-Syn (C), (E), (G), (I) and α-Syn with N-terminal acetylation (D), (F), (H), (J). Three types of oligomers are classified by Gaussian fitting, and Oligomer I, II, III are marked by pink, green and blue solid lines, respectively. (K), (L) The percentage change with incubation time of under-curve area for Oligomer I and II, and the solid line is fitted with the method of least squares. Data point in 24 h incubation of N-terminally acetylated α-Syn sample is not shown due to the small number of captured molecules.

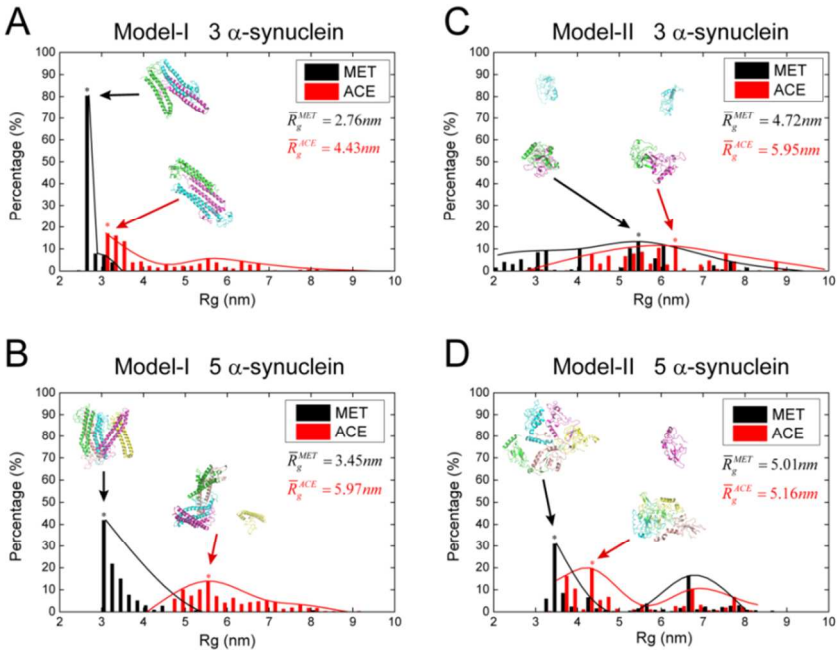

Figure 2. Radius of gyration of multiple α-Syn oligomerization in REMD simulations. MET represents the wild-type α-Syn, while ACE is short for the N-terminal acetylation. (A) and (B) The radius of gyration distribution of 3 and 5 α-Syn of model-I, starting with the crystal structure (PDB: 1XQ8) with two α-helices in each α-Syn, respectively. (C) and (D) The radius of gyration distribution of 3 and 5 α-Syn of model-II, starting with a random coil based on the sequence in each α-Syn, respectively. The average values of radius of gyrations are shown as $\overline{R}_g^{MET}$ and $\overline{R}_g^{ACE}$, respectively. The insets illustrate the oligomerization structures of the most frequently appearing states. The solid lines are the envelope of the corresponding distribution histograms.

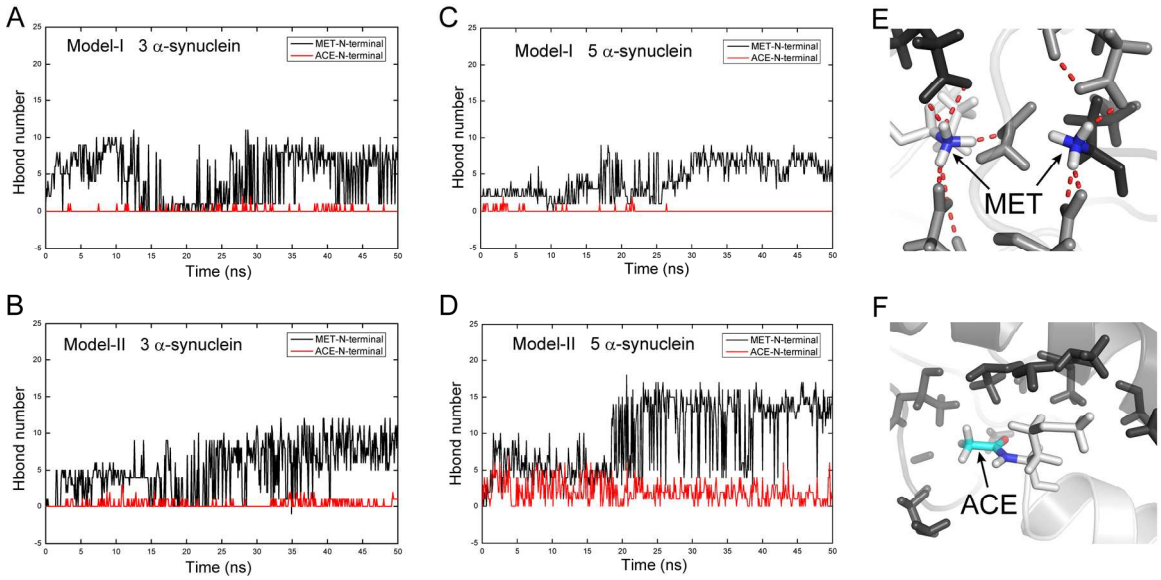

Figure 3. N-terminal acetylation weakens the oligomerization of α-Syn by reducing the H-bond numbers between the acetylated N-terminus and residues in α-Syn belonging to other α-Syn sequences. (A) and (B) The H-bond number between the N-terminal end and other residues belonging to other α-Syn sequences of Model-I and Model-II with 3 α-Syns, respectively. (C) and (D) The H-bond number between the N-terminal end and other residues belonging to other α-Syn sequences of Model-I and Model-II with 5 α-Syns, respectively. MET represents the wild-type α-Syn, while ACE is short for the N-terminal acetylation. (E) Illustration of H-bond network between the WT N-terminal end and residues in other α-Syn molecules. The H-bonds are represented by red dashed lines. (F) Illustration of acetylated N-terminal interactions with residues in other α-Syn molecules, showing that there is nearly no H-bond formation between the acetylated N-terminal end and residues in other α-Syn molecules.

References:

1. Maroteaux, L.; Campanelli, J. T.; Scheller, R. H., Synuclein - a Neuron-Specific Protein Localized to the Nucleus and Presynaptic Nerve-Terminal. *J Neurosci* **1988,** *8* (8), 2804-2815.

2. Jensen, P. H.; Nielsen, M. S.; Jakes, R.; Dotti, C. G.; Goedert, M., Binding of alpha-synuclein to brain vesicles is abolished by familial Parkinson's disease mutation. *J Biol Chem* **1998,** *273* (41), 26292-4.

3. Wang, C.; Zhao, C.; Li, D.; Tian, Z.; Lai, Y.; Diao, J.; Liu, C., Versatile Structures of alpha-Synuclein. *Front Mol Neurosci* **2016,** *9*, 48.

4. Diao, J.; Burre, J.; Vivona, S.; Cipriano, D. J.; Sharma, M.; Kyoung, M.; Sudhof, T. C.; Brunger, A. T., Native alpha-synuclein induces clustering of synaptic-vesicle mimics via binding to phospholipids and synaptobrevin-2/VAMP2. *Elife* **2013,** *2*, e00592.

5. Lai, Y.; Kim, S.; Varkey, J.; Lou, X.; Song, J. K.; Diao, J.; Langen, R.; Shin, Y. K., Nonaggregated alpha-Synuclein Influences SNARE-Dependent Vesicle Docking via Membrane Binding. *Biochemistry* **2014,** *53* (24), 3889-96.

6. Goedert, M., Alpha-synuclein and neurodegenerative diseases. *Nat Rev Neurosci* **2001,** *2* (7), 492-501.

7. Kruger, R.; Kuhn, W.; Muller, T.; Woitalla, D.; Graeber, M.; Kosel, S.; Przuntek, H.; Epplen, J. T.; Schols, L.; Riess, O., Ala30Pro mutation in the gene encoding alpha-synuclein in Parkinson's disease. *Nature genetics* **1998,** *18* (2), 106-8.

8. Polymeropoulos, M. H.; Lavedan, C.; Leroy, E.; Ide, S. E.; Dehejia, A.; Dutra, A.; Pike, B.; Root, H.; Rubenstein, J.; Boyer, R.; Stenroos, E. S.; Chandrasekharappa, S.; Athanassiadou, A.; Papapetropoulos, T.; Johnson, W. G.; Lazzarini, A. M.; Duvoisin, R. C.; Di Iorio, G.; Golbe, L. I.; Nussbaum, R. L., Mutation in the alpha-synuclein gene identified in families with Parkinson's disease. *Science* **1997,** *276* (5321), 2045-7.

9. Zarranz, J. J.; Alegre, J.; Gomez-Esteban, J. C.; Lezcano, E.; Ros, R.; Ampuero, I.; Vidal, L.; Hoenicka, J.; Rodriguez, O.; Atares, B.; Llorens, V.; Gomez Tortosa, E.; del Ser, T.; Munoz, D. G.; de Yebenes, J. G., The new mutation, E46K, of alpha-synuclein causes Parkinson and Lewy body dementia. *Annals of neurology* **2004,** *55* (2), 164-73.

10. Chartier-Harlin, M. C.; Kachergus, J.; Roumier, C.; Mouroux, V.; Douay, X.; Lincoln, S.; Levecque, C.; Larvor, L.; Andrieux, J.; Hulihan, M.; Waucquier, N.; Defebvre, L.; Amouyel, P.; Farrer, M.; Destee, A., Alpha-synuclein locus duplication as a cause of familial Parkinson's disease. *Lancet* **2004,** *364* (9440), 1167-9.

11. Singleton, A. B.; Farrer, M.; Johnson, J.; Singleton, A.; Hague, S.; Kachergus, J.; Hulihan, M.; Peuralinna, T.; Dutra, A.; Nussbaum, R.; Lincoln, S.; Crawley, A.; Hanson, M.; Maraganore, D.; Adler, C.; Cookson, M. R.; Muenter, M.; Baptista, M.; Miller, D.; Blancato, J.; Hardy, J.; Gwinn-Hardy, K., alpha-Synuclein locus triplication causes Parkinson's disease. *Science* **2003,** *302* (5646), 841.

12. Bucciantini, M.; Giannoni, E.; Chiti, F.; Baroni, F.; Formigli, L.; Zurdo, J.; Taddei, N.; Ramponi, G.; Dobson, C. M.; Stefani, M., Inherent toxicity of aggregates implies a common mechanism for protein misfolding diseases. *Nature* **2002,** *416* (6880), 507-11.

13. Conway, K. A.; Lee, S. J.; Rochet, J. C.; Ding, T. T.; Harper, J. D.; Williamson, R. E.; Lansbury, P. T., Jr., Accelerated oligomerization by Parkinson's disease linked alpha-synuclein mutants. *Annals of the New York Academy of Sciences* **2000,** *920*, 42-5.

14. Goldberg, M. S.; Lansbury, P. T., Jr., Is there a cause-and-effect relationship between alpha-synuclein fibrillization and

Parkinson's disease? *Nature cell biology* **2000,** *2* (7), E115-9.

15. Theillet, F. X.; Binolfi, A.; Bekei, B.; Martorana, A.; Rose, H. M.; Stuiver, M.; Verzini, S.; Lorenz, D.; van Rossum, M.; Goldfarb, D.; Selenko, P., Structural disorder of monomeric alpha-synuclein persists in mammalian cells. *Nature* **2016,** *530* (7588), 45-50.

16. Burre, J.; Vivona, S.; Diao, J.; Sharma, M.; Brunger, A. T.; Sudhof, T. C., Properties of native brain alpha-synuclein. *Nature* **2013,** *498* (7453), E4-6; discussion E6-7.

17. Maltsev, A. S.; Ying, J.; Bax, A., Impact of N-terminal acetylation of alpha-synuclein on its random coil and lipid binding properties. *Biochemistry* **2012,** *51* (25), 5004-13.

18. Dikiy, I.; Eliezer, D., N-terminal acetylation stabilizes N-terminal helicity in lipid- and micelle-bound alpha-synuclein and increases its affinity for physiological membranes. *J Biol Chem* **2014,** *289* (6), 3652-65.

19. Kang, L.; Moriarty, G. M.; Woods, L. A.; Ashcroft, A. E.; Radford, S. E.; Baum, J., N-terminal acetylation of alpha-synuclein induces increased transient helical propensity and decreased aggregation rates in the intrinsically disordered monomer. *Protein science : a publication of the Protein Society* **2012,** *21* (7), 911-7.

20. Iyer, A.; Roeters, S. J.; Schilderink, N.; Hommersom, B.; Heeren, R. M.; Woutersen, S.; Claessens, M. M.; Subramaniam, V., The Impact of N-terminal Acetylation of alpha-Synuclein on Phospholipid Membrane Binding and Fibril Structure. *J Biol Chem* **2016,** *291* (40), 21110-21122.

21. Rossetti, G.; Musiani, F.; Abad, E.; Dibenedetto, D.; Mouhib, H.; Fernandez, C. O.; Carloni, P., Conformational ensemble of human alpha-synuclein physiological form predicted by molecular simulations. *Phys Chem Chem Phys* **2016,** *18* (8), 5702-5706.

22. Hu, R.; Diao, J.; Li, J.; Tang, Z.; Li, X.; Leitz, J.; Long, J.; Liu, J.; Yu, D.; Zhao, Q., Intrinsic and membrane-facilitated alpha-synuclein oligomerization revealed by label-free detection through solid-state nanopores. *Sci Rep* **2016,** *6*, 20776.

23. Yusko, E. C.; Prangkio, P.; Sept, D.; Rollings, R. C.; Li, J.; Mayer, M., Single-particle characterization of Abeta oligomers in solution. *ACS Nano* **2012,** *6* (7), 5909-19.

24. Talaga, D. S.; Li, J., Single-molecule protein unfolding in solid state nanopores. *J Am Chem Soc* **2009,** *131* (26), 9287-97.

25. Kummer, M. P.; Heneka, M. T., Truncated and modified amyloid-beta species. *Alzheimers Res Ther* **2014,** *6* (3), 28.

26. Marotta, N. P.; Lin, Y. H.; Lewis, Y. E.; Ambroso, M. R.; Zaro, B. W.; Roth, M. T.; Arnold, D. B.; Langen, R.; Pratt, M. R., O-GlcNAc modification blocks the aggregation and toxicity of the protein alpha-synuclein associated with Parkinson's disease. *Nat Chem* **2015,** *7* (11), 913-20.

27. de Oliveira, R. M.; Vicente Miranda, H.; Francelle, L.; Pinho, R.; Szego, E. M.; Martinho, R.; Munari, F.; Lazaro, D. F.; Moniot, S.; Guerreiro, P.; Fonseca, L.; Marijanovic, Z.; Antas, P.; Gerhardt, E.; Enguita, F. J.; Fauvet, B.; Penque, D.; Pais, T. F.; Tong, Q.; Becker, S.; Kugler, S.; Lashuel, H. A.; Steegborn, C.; Zweckstetter, M.; Outeiro, T. F., The mechanism of sirtuin 2-mediated exacerbation of alpha-synuclein toxicity in models of Parkinson disease. *PLoS Biol* **2017,** *15* (3), e2000374.

28. Arnesen, T., Towards a Functional Understanding of Protein N-Terminal Acetylation. *PLoS Biology* **2011,** *9* (5).

29. Trexler, A. J.; Rhoades, E., N‐terminal acetylation is critical for forming α‐helical oligomer of α‐synuclein. *Protein Science* **2012,** *21* (5), 601-605.

30. Bartels, T.; Ahlstrom, L. S.; Leftin, A.; Kamp, F.; Haass, C.; Brown, M. F.; Beyer, K., The N-Terminus of the Intrinsically Disordered Protein α-Synuclein Triggers Membrane Binding and Helix Folding. *Biophys J* **2010,** *99* (7), 2116-2124.

31. Shankar, G. M.; Li, S.; Mehta, T. H.; Garcia-Munoz, A.; Shepardson, N. E.; Smith, I.; Brett, F. M.; Farrell, M. A.; Rowan, M. J.; Lemere, C. A.; Regan, C. M.; Walsh, D. M.; Sabatini, B. L.; Selkoe, D. J., Amyloid-beta protein dimers isolated directly from Alzheimer's brains impair synaptic plasticity and memory. *Nat Med* **2008,** *14* (8), 837-42.

32. Conway, K. A.; Lee, S.-J.; Rochet, J.-C.; Ding, T. T.; Williamson, R. E.; Lansbury, P. T., Acceleration of oligomerization, not fibrillization, is a shared property of both α-synuclein mutations linked to early-onset Parkinson's disease: Implications for pathogenesis and therapy. *Proceedings of the National Academy of Sciences* **2000,** *97* (2), 571-576.

33. Winner, B.; Jappelli, R.; Maji, S. K.; Desplats, P. A.; Boyer, L.; Aigner, S.; Hetzer, C.; Loher, T.; Vilar, M.; Campioni, S.; Tzitzilonis, C.; Soragni, A.; Jessberger, S.; Mira, H.; Consiglio, A.; Pham, E.; Masliah, E.; Gage, F. H.; Riek, R., In vivo demonstration that α-synuclein oligomers are toxic. *Proceedings of the National Academy of Sciences* **2011,** *108* (10), 4194-4199.

34. Ghosh, D.; Mehra, S.; Sahay, S.; Singh, P. K.; Maji, S. K., α-synuclein aggregation and its modulation. *International journal of biological macromolecules* **2016**.

35. Li, D. C.; Ji, B. H.; Hwang, K.; Huang, Y. G., Crucial Roles of the Subnanosecond Local Dynamics of the Flap Tips in the Global Conformational Changes of HIV-1 Protease. *Journal of Physical Chemistry B* **2010,** *114* (8), 3060-3069.

36. Li, D. C.; Ji, B. H.; Hwang, K. C.; Huang, Y. G., Strength of Hydrogen Bond Network Takes Crucial Roles in the Dissociation Process of Inhibitors from the HIV-1 Protease Binding Pocket. *Plos One* **2011,** *6* (4).

37. Xu, C. J.; Li, D. C.; Cheng, Y.; Liu, M.; Zhang, Y. W.; Ji, B. H., Pulling out a peptide chain from beta-sheet crystallite: Propagation of instability of H-bonds under shear force. *Acta Mech Sinica-Prc* **2015,** *31* (3), 416-424.

38. Yoon, J.; Jang, S.; Lee, K.; Shin, S., Simulation Studies on the Stabilities of Aggregates Formed by Fibril-Forming Segments of α-Synuclein. *Journal of Biomolecular Structure and Dynamics* **2009,** *27* (3), 259-269.

39. Rojas, A. V.; Maisuradze, N.; Kachlishvili, K.; Scheraga, H.; Maisuradze, G. G., Elucidating important sites and the mechanism for amyloid fibril formation by coarse-grained molecular dynamics. *ACS Chemical Neuroscience* **2016**.

40. Ulmer, T. S.; Bax, A.; Cole, N. B.; Nussbaum, R. L., Structure and Dynamics of Micelle-bound Human α-Synuclein. *Journal of Biological Chemistry* **2005,** *280* (10), 9595-9603.

41. Vermaas, J. V.; Tajkhorshid, E., Conformational heterogeneity of α-synuclein in membrane. *Biochimica et biophysica acta* **2014,** *1838* (12), 3107-3117.

42. Patriksson, A.; van der Spoel, D., A temperature predictor for parallel tempering simulations. *Phys Chem Chem Phys* **2008,** *10* (15), 2073-2077.

43. Swendsen, R. H.; Wang, J.-S., Replica Monte Carlo Simulation of Spin-Glasses. *Physical Review Letters* **1986,** *57* (21), 2607-2609.

44. Lei, H.; Duan, Y., Improved sampling methods for molecular simulation. *Current Opinion in Structural Biology* **2007,** *17* (2), 187-191.

45. Klauda, J. B.; Monje, V.; Kim, T.; Im, W., Improving the CHARMM force field for polyunsaturated fatty acid chains. *The journal of physical chemistry. B* **2012,** *116* (31), 9424-9431.

46. Klauda, J. B.; Venable, R. M.; Freites, A. J.; O'Connor, J. W.; Tobias, D. J.; Mondragon-Ramirez, C.; Vorobyov, I.; MacKerell, A. D.; Pastor, R. W., Update of the CHARMM all-atom additive force field for lipids: validation on six lipid types. *The journal of physical chemistry. B* **2010,** *114* (23), 7830-7843.

47. Still, C. W.; Tempczyk, A.; Hawley, R. C.; Hendrickson, T., Semianalytical treatment of solvation for molecular mechanics and dynamics. *Journal of the American Chemical Society* **1990,** *112* (16), 6127-6129.

48. Tao, W. W.; Yoon, G.; Cao, P. H.; Eom, K.; Park, H. S., beta-sheet-like formation during the mechanical unfolding of prion protein. *Journal of Chemical Physics* **2015,** *143* (12).

49. Raman, E. P.; Takeda, T.; Klimov, D. K., Molecular Dynamics Simulations of Ibuprofen Binding to A beta Peptides. *Biophys J* **2009,** *97* (7), 2070-2079.

50. Izadi, S.; Aguilar, B.; Onufriev, A. V., Protein–Ligand Electrostatic Binding Free Energies from Explicit and Implicit Solvation. *Journal of Chemical Theory and Computation* **2015,** *11* (9), 4450-4459.

51. Liu, Y.; Haddadian, E.; Sosnick, T. R.; Freed, K. F.; Gong, H., A Novel Implicit Solvent Model for Simulating the Molecular Dynamics of RNA. *Biophys J* **2013,** *105* (5), 1248-1257.

52. Razzokov, J.; Naderi, S.; van der Schoot, P., Prediction of the structure of a silk-like protein in oligomeric states using explicit and implicit solvent models. *Soft Matter* **2014,** *10* (29), 5362-5374.

53. Hess, B., P-LINCS: A Parallel Linear Constraint Solver for Molecular Simulation. *Journal of Chemical Theory and Computation* **2008,** *4* (1), 116-122.

54. Abraham, M.; Murtola, T.; Schulz, R.; Páll, S.; Smith, J. C.; Hess, B.; Lindahl, E., GROMACS: High performance molecular simulations through multi-level parallelism from laptops to supercomputers. *SoftwareX* **2015,** *1*, 19-25.

55. Van Der Spoel, D.; Lindahl, E.; Hess, B.; Groenhof, G.; Mark, A. E.; Berendsen, H. J., GROMACS: fast, flexible, and free. *Journal of computational chemistry* **2005,** *26* (16), 1701-1718.

56. Qin, S. B.; Zhou, H. X., Atomistic Modeling of Macromolecular Crowding Predicts Modest Increases in Protein Folding and Binding Stability. *Biophys J* **2009,** *97* (1), 12-19.

57. Li, X. Q.; Hu, R.; Li, J.; Tong, X.; Diao, J. J.; Yu, D. P.; Zhao, Q., Non-sticky translocation of bio-molecules through Tween 20-coated solid-state nanopores in a wide pH range. *Applied Physics Letters* **2016,** *109* (14).

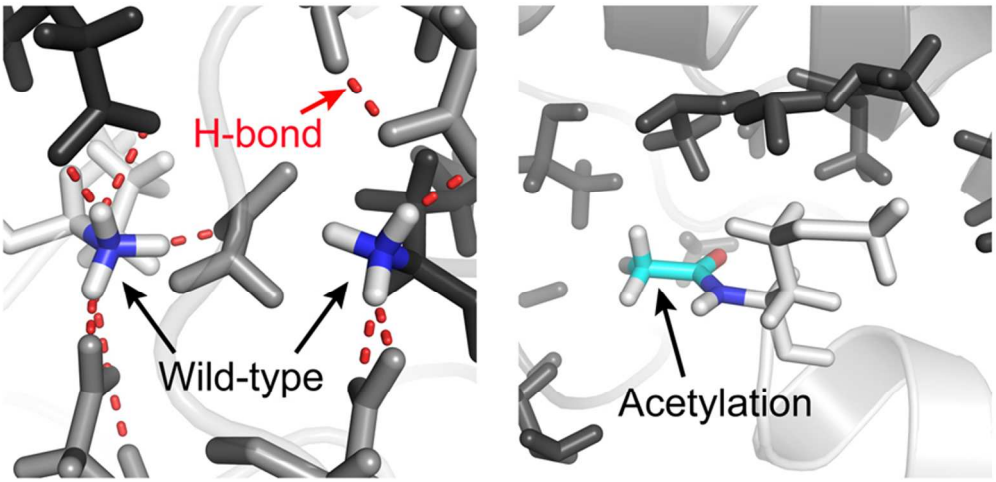

80x39mm (300 x 300 DPI)